Direct numerical simulation of a turbulent boundary layer over an oscillating wall

Yudhistira, Indra; Skote, Martin

2011

Yudhistira, I., & Skote, M. (2011). Direct numerical simulation of a turbulent boundary layer over an oscillating wall. Journal of turbulence, 12(9), 1-17.

https://hdl.handle.net/10356/101617

https://doi.org/10.1080/14685248.2010.538397

Vol. 00, No. 00, 200x, 2–18

RESEARCH ARTICLE

Direct Numerical Simulation of a Turbulent Boundary Layer over an Oscillating Wall

Indra Yudhistira and Martin Skote*

School of Mechanical & Aerospace Engineering
Nanyang Technological University
50 Nanyang Avenue, North Spine N3.2-02-34 Singapore 639798
(*Received 00 Month 200x; final version received 00 Month 200x*)

Direct Numerical Simulations have been performed to study the effect of a partially oscillating wall on the turbulent boundary layer. Even though the Reynolds number is three times lower than in previous experimental investigations, many of the characteristic flow features are confirmed. The drag reduction is of the same magnitude as for higher Reynolds number flows, and the spatial development follows closely earlier experimental findings. The reduction of Reynolds shear stress is more pronounced than the decrease in streamwise and normal velocity fluctuations. In addition, comparisons are made with earlier numerical studies of channel flow. The sensitivity of the Reynolds shear stress on the time allowed for statistics collection is scrutinised, and the discrepancy in results from earlier experiments are thus explained.

Keywords: Direct Numerical Simulation; Turbulent Boundary Layer; Oscillating Wall

1. Introduction

Ever since Jung et al. [1] (inspired by earlier experiments and simulations of three-dimensional wall-bounded flows) in a short paper presented results from a DNS of a channel flow subjected to oscillatory spanwise wall motion, a number of investigations have been devoted to explain and optimise the skin friction reduction. Channel flow has been the geometry of choice for numerical studies, using Direct Numerical Simulations (DNS), while boundary layer flow is more common in the experimental work in this area of research.

Baron and Quadrio [2] were the next researchers to report from a channel flow simulation with a spanwise oscillating wall. They presented more details of the flow; the scaling of velocity profiles and Reynolds stresses, as well as the effect of oscillation on the turbulent energy budget.

Choi et al. [3] performed DNS of both channel and pipe flow with oscillating walls and offer a phenomenological analysis of the mechanism of the drag reduction, related to high speed fluid penetrating beneath the low-speed streaks.

Quadrio and Ricco [4] conducted DNS of channel flow and analysed the transient behaviour in the first few cycles of wall oscillations. They also noted that the spanwise velocity profile follows the analytical profile given by second Stokes problem. In another paper by Quadrio and Ricco [5], much of the earlier DNS and experiments were reviewed and discrepancies regarding the resulting drag reduction were explained. The influence of the oscillation parameters, such as the amplitude and frequency, on the drag reduction was investigated.

*Corresponding author. Email: mskote@ntu.edu.sg

The later paper by Xu and Huang [6] offers an explanation of the drag reduction from the transport equations of the Reynolds stresses. In the recent paper by Ricco and Quadrio [7], a parameter based on the action of the oscillating Stokes layer, is shown to give a linear relation with the resulting drag reduction. The parameter will be discussed later in this section.

In most of the numerical work, the wall oscillation is imposed through a wall velocity (W) in the spanwise direction in the form of

$$W = W_m \sin\left(\frac{2\pi t}{T}\right), \tag{1}$$

where W_m is the maximum wall velocity and T is the period of oscillation which is related to the frequency (f) through $f = 1/T$.

There are many benefits of choosing the channel flow geometry for numerical work. Aside from the simpler geometry and boundary conditions (compared to boundary layer flows), a crucial advantage is that the turbulence statistics are easily calculated by averaging in both the streamwise and spanwise directions. In the boundary layer case however, the inhomogeneous streamwise direction makes temporal statistics necessary. While this is relatively straightforward in steady (statistically) flows, the oscillating wall impose unsteady mean flow (in the spanwise direction), and the need for phase averaging in this case makes certain statistics unavailable (such as w_{rms}) when performing DNS (due to limited computing resources), albeit they can be readily obtained experimentally. Therefore, the investigations of boundary layer flow with an oscillating wall have so far been restricted to experimental work.

Laadhari et al. [8] were the first who confirmed that Jung's results also applied to the boundary layer flow. Since then, most of the experimental investigations have in fact been focused on the boundary layer, see e.g. [9–16]. The wall oscillation in the experiments is often implemented via the maximum wall displacement D_m, which is related to maximum wall velocity through

$$D_m = W_m T/\pi. \tag{2}$$

Experimental findings regarding the spatial development of the drag reduction can be found in the works of Choi et al. [10], who reported a drag reduction upstream of the oscillating part of the wall. Also Bogard et al. [11] and Ricco & Wu [15] observed the downstream development of the drag reduction but no upstream influence could be detected.

The reduction of Reynolds stresses in boundary layer flows over an oscillating wall has been quantified by Laadhari et al. [8], Choi & Clayton [12], Trujillo et al. [9] and Ricco & Wu [15]. The exact numbers of the decrease in intensities will be discussed later in this paper (section 3.2), but the general trend is that the Reynolds shear stress reduces more than the streamwise and normal velocity fluctuations.

In the experiments conducted by Bogard et al. [11], the Reynolds number based on momentum thickness varied from 500 to 1500, and no dependency on the Reynolds number on the drag reduction could be detected. They claim that the drag reduction is not dependent on the oscillation frequency (T) nor on the oscillation amplitude (D_m), but rather the peak wall speed (W_m). The dependency of drag reduction on only W_m has also been suggested by Choi & Graham [17], Karniadakis & Choi [18] and Trujillo et al. [9], among others. However, later investigations have shown that both the peak wall speed (or amplitude since they are related through equation (2)) and period (or frequency) together determines the

drag reduction. Ricco and Quadrio [7] have suggested a parameter S that varies linearly with the drag reduction according to

$$\mathrm{DR}(\%) = S_1 S + S_2, \tag{3}$$

where $S_1 = 135.11$ and $S_2 = -0.85$ are two constants determined by fitting the linear expression to experimental and numerical drag reduction data. The expression for dimensionless drag reduction scaling parameter S is given by:

$$S = \frac{a_m^+ l_w^+}{W_m^+} = 2\sqrt{\frac{\pi}{T^+}} \ln\left(\frac{W_m^+}{W_{th}^+}\right) \exp\left(-l_a^+ \sqrt{\pi/T^+}\right). \tag{4}$$

The + superscript denotes variables in inner (wall) scaling.

Here a_m^+ and l_w^+ represent the scaled maximum acceleration of the Stokes layer, and the scaled wall-normal distance respectively, while W_m^+ is the scaled maximum wall velocity. The scaled period of wall oscillation is given by T^+, while W_{th}^+ denotes threshold spanwise velocity, and l_a^+ is scaled wall-normal distance at which a_m^+ is computed. The parameters l_a^+ and W_{th}^+ have been determined by maximizing the correlation coefficient between the drag reduction data and S. The value of the parameters given in [7] are: $l_a^+ = 6.2$ and $W_{th}^+ = 1.7$.

The pipe flow has also been observed to exhibit drag reduction when the wall undergoes oscillation. The DNS performed by Quadrio & Sibilla [19] showed evidence of the lateral displacement of low-speed streaks with respect to the streamwise vortices. They compare their results with the higher Reynolds number oscillating pipe flow experiments conducted by Choi & Graham [17].

Furthermore, for the boundary layer geometry, some numerical work has been performed on the impulsively started wall motion, and on boundary layer flows with constant wall motion resulting in a three-dimensional boundary layer flow. See e.g. the work by Kannepalli & Piomelli [20] which we will make comparison with in the present paper.

The present paper is the first reported work (according to the authors knowledge) on DNS of a turbulent boundary layer over an oscillating wall, and is organized as follows. In section 2 the numerical method and simulation related issues are discussed. The results are presented in section 3. In total four simulations have been performed. Both the unmanipulated (non-oscillating) turbulent boundary layer and the boundary layer flowing over an oscillating wall have been conducted using two different resolutions. Our results are compared with other investigations; both with experiments (of the boundary layer flow) and DNS (of the channel flow). Lastly, conclusions are drawn in section 4.

2. Numerical method and simulation parameters

The simulations of turbulent boundary layer flows over a wall that oscillates have been performed using a code developed at KTH, Stockholm [21]. The code used for the simulations has been used extensively over the years, see references in [21]. An outline of the numerical scheme is presented in section 2.1, the various parameters used and the resolution are presented next in section 2.2. The code has been modified to allow for an oscillating motion of parts of the wall, and the implementation of the wall motion is presented in section 2.3.

2.1. *Numerical Scheme*

A pseudo-spectral method is employed, with Fourier discretization used in the streamwise and spanwise directions, and Chebyshev polynomials in the wall-normal direction. The simulations start with a laminar boundary layer at the inflow which is triggered to transition by a random volume force near the wall. A fringe region is added at the end of the computational domain to enable simulations of spatially developing flows. In this region the flow is forced from the outflow of the physical domain to the inflow. In this way the physical domain and the fringe region together satisfy periodic boundary conditions. The implementation is done by adding a volume force

$$F_i = \lambda(x)(\widetilde{u}_i - u_i) \tag{5}$$

to the Navier-Stokes equations,

$$\frac{\partial u_i}{\partial t} + u_j \frac{\partial u_i}{\partial x_j} = -\frac{1}{\rho}\frac{\partial p}{\partial x_i} + \nu \frac{\partial^2 u_i}{\partial x_j^2} + F_i \tag{6}$$

The force F_i acts only in the fringe region. $\widetilde{u}_i$ is the laminar inflow velocity profile the solution u_i is forced to and $\lambda(x)$ is the strength of the forcing. The form of the fringe function is designed to have minimal upstream influence and is given by

$$\lambda(x) = \lambda_{max} f(x) \tag{7}$$

with

$$f(x) = S\left(\frac{x - x_{start}}{\Delta x_{rise}}\right) - S\left(\frac{x - x_{end}}{\Delta x_{fall}} + 1\right). \tag{8}$$

Here λ_{max} is the maximum strength of the fringe, x_{start} and x_{end} denotes the spatial extent of the region where the fringe is non-zero, Δx_{rise} and Δx_{fall} are the rise and fall distance of the fringe function respectively. $S(x)$ is a continuous step function that rises from zero for negative x to unity for $x \geq 1$. The expression of $S(x)$, which has the advantage of having continuous derivatives of all orders is,

$$S(x) = \begin{cases} 0, & x \leq 0, \\ 1/(1 + e^{(1/(x-1)+1/x)}), & 0 < x < 1, \\ 1, & x \geq 1. \end{cases} \tag{9}$$

A schematic example of the $f(x)$ profile is given in Figure 2.1. The function $f(x)$ is also used two more times in the implementation of the wall oscillation described in section 2.3.

The time integration is performed using a third-order Runge-Kutta-scheme for the non-linear terms and a second-order Crank-Nicolson method for the linear terms. A 3/2-rule is applied to remove aliasing errors from the evaluation of the non-linear terms when calculating FFTs in the wall parallel plane.

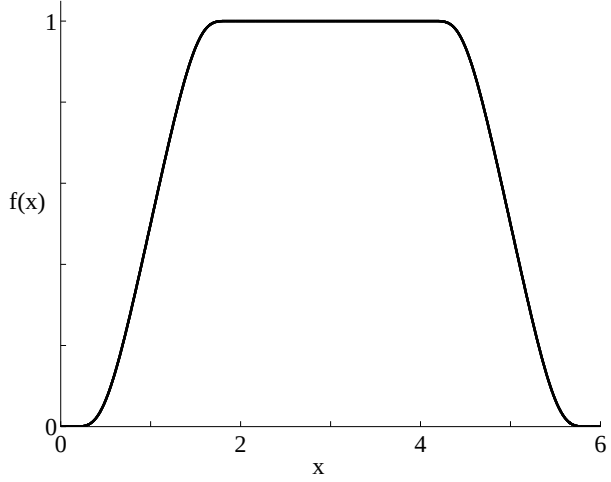

Figure 1. Schematic picture of $f(x)$, equation (8). Here $x_{start} = 0$;$x_{end} = 6$; $\Delta x_{rise} = 2$ and $\Delta x_{fall} = 2$.

2.2. *Numerical parameters*

All quantities are non-dimensionalized by the freestream velocity (U) and the displacement thickness (δ^*) at the starting position of the simulation ($x = 0$), where the flow is laminar. The Reynolds number is set by specifying $Re_{\delta^*} = U\delta^*/\nu$ at $x = 0$. In all the simulations presented here, $Re_{\delta^*} = 450$.

A laminar Blasius boundary layer profile is introduced in the very beginning of the computational box at $x = 0$. Laminar-turbulent transition is triggered by a random volume force near the wall at $x = 5$ downstream. This triggering action is caused by a local volume force normal to the surface which is given by

$$F_2 = e^{[(x-t_{x0})/t_{xsc}]^2-(y/t_{ysc})^2} f(z,t) \tag{10}$$

where

$$f(z,t) = t_{ampt}[(1 - b(t))h^i(z) + b(t)h^{i+1}(z)] \tag{11}$$

with $i = \mathrm{int}(t/t_{dt})$, $b(t) = 3p^2 - 2p^3$, $p = t/t_{dt} - i$. The h^i are Fourier series with amplitude of unity, using 40 random coefficients. The maximum amplitude of the forcing is given by $t_{ampt} = 0.4$, the length scales of the trip $t_{xsc} = 4.0$ and $t_{ysc} = 2.0$ and origin of trip in streamwise direction $t_{x0} = 5.0$. A time interval $t_{dt} = 1.0$ is used between the changes of the random part of the trip.

The technique described above has been used in a number of turbulent boundary layer simulations, see e.g. [22–24], and recently in [25].

The computational box is 600 in simulation length units (δ^*) long (including 100 units for the fringe), 30 units high and 34 units wide. The parameters of the fringe are $\lambda_{max} = 1.0$, $x_{start} = 500$, $x_{end} = 600$, $x_{rise} = 60$ and $x_{fall} = 40$.

As the fringe starts at $x = 500$, we will present results only up to $x = 470$ to avoid any upstream influence of the fringe. The transition region is roughly between $x = 5$ and $x = 150$. Thus, the region of a fully developed turbulent boundary layer, free from any influence of the numerical method, is $x = 150 - 470$. The Reynolds number based on the momentum thickness (Re_θ) is varying between 418 and 750 in this region for the unmanipulated (non-oscillating) boundary layer. In inner scaling based on the friction velocity at $x = 250$, the region $x = 150 - 470$ amounts to about 7200 wall units.

All parameter values presented this far were used unchanged for all four simu-

lations presented in this paper. The two resolutions used for the simulations were 600 and 800 modes in streamwise direction, 201 modes in wall-normal direction (equal for both cases), 128 and 144 modes in the spanwise direction.

Of the two different resolutions used, most of the results presented were obtained from the simulations with the higher resolution. The two resolutions are denoted RES1 and RES2 respectively and are summerized in Table 1, together with parameters for the two oscillating cases. The parameters NX, NZ, NY refer to the number of modes in the streamwise, spanwise and wall-normal directions respectively.

Note that unless otherwise stated, the + superscript indicates that the quantity is made non-dimensional with the friction velocity of the unmanipulated boundary layer (the reference case), denoted u_τ^0, and the kinematic viscosity (ν). Thus, the resolution in viscous length units (+) in Table 1 is given in reference wall units. Using the friction velocity from the oscillating boundary layer (actual u_τ) would give much finer resolution (in actual wall units) since the friction velocity has decreased for that case.

2.3. *Implementation of Wall Oscillation*

A slight modification is made to the code to accommodate for wall oscillation in the form of equation (1). The wall oscillation is applied in the spanwise direction at a particular region in streamwise direction. Therefore, a profile function $f(x)$ is utilized to serve as a filter to select the domain where the oscillation takes place.

The form of this boundary condition is given by

$$w|_{y=0} = W_m f(x) \sin[\omega(t - t_{start})] g(t) \tag{12}$$

where $f(x)$ is the same profile function as used for fringe region, see equation (8) and Figure 2.1, with x_{start}, x_{end}, x_{rise} and x_{fall} set to 250, 450, 10 and 10 respectively. The parameter ω is the angular frequency of the wall oscillation, which is related to the period through $\omega = 2\pi/T$.

The function $g(t)$ is the temporal version of $f(x)$ and is written as,

$$g(t) = S\left(\frac{t - t_{start}}{\Delta t_{rise}}\right) - S\left(\frac{t - t_{end}}{\Delta t_{fall}} + 1\right), \tag{13}$$

with $S(t)$ is the same continuous step function as $S(x)$ (equation 9) which is in this case applied in the time domain. Here t_{start} and t_{end} denote the temporal extent of the time when the oscillation is non-zero and Δt_{rise} and Δt_{fall} are the rise and fall time respectively, which are in effect the ramp-up and ramp-down time for the oscillation. The expression (12) for the wall velocity thus provides a smooth transition from non-moving wall to oscillating wall both spatially (x) and temporally (t).

Note that the ramp-up is only used at the very beginning of the oscillations (over a time of Δt_{rise}), and t_{end} is set to an arbitrarily large number. Only if the effects of stopping the oscillations is of interest, will the parameter t_{end} and Δt_{fall} in equation (13) be used. The start of the oscillation was set at $t_{start} = 3000$ in time units (δ^*/U), i.e. the flow with speed U has convected five times through the computational box before the wall starts to oscillate. The parameter Δt_{rise} is set to 10, thus it is only approximately one tenth of the period of the oscillation.

The parameter W_m is the maximum wall speed and is given (in wall units) in Table (1) for the two cases, together with the oscillation period in wall units which

Table 1. The two resolutions and the oscillation parameters.

Resolution	NX	NZ	NY	ΔX^+	ΔZ^+	ΔY^+_{min}	W^+_m	T^+	D^+_m
RES1	640	128	201	20	5.8	0.04	27	100	859
RES2	800	144	201	16	5.1	0.04	18	100	573

in both cases is $T^+ = Tu_\tau^2/\nu = 100$. Also the maximum wall displacement, which is related to the other two parameters through expression (2), is shown in Table (1).

3. Results

In section 3.1 the two cases RES1 and RES2, with and without wall oscillation will be discussed. A resolution check for the non-oscillating case is done by comparing RES1 and RES2. The early stages of wall oscillation is described for the case with a higher spanwise wall velocity but lower resolution (RES1). The downstream development of the drag reduction is described for the RES2 case. In section 3.2 the long term statistics are discussed solely from the RES2 case, and in section 3.3 the budget for the longitudinal Reynolds stress is presented.

3.1. *General flow features*

In the first case (RES1) the magnitude of the wall oscillation was set to $W_m = 1.286$, which corresponds to $W_m^+ = 27$. The period is set to $T^+ = 100$. The oscillation part of the wall is located between $x = 250$ and $x = 450$, and is thus 200 simulation units (δ^*) long, including the spatial ramp-up and ramp-down distances of 10 units each. Only the developing (in time and space) skin friction will be presented for this case, while other statistics are presented from the RES2 case.

The friction coefficient is defined as

$$C_f = 2\left(\frac{u_\tau}{U_\infty}\right)^2, \tag{14}$$

where the friction velocity u_τ is calculated from the mean streamwise velocity gradient at the wall:

$$u_\tau \equiv \sqrt{\nu \left.\frac{\partial u}{\partial y}\right|_{y=0}} \tag{15}$$

In Figure 2 the skin friction coefficient is shown as a function of the streamwise coordinate (x) after two, four and six oscillations, together with the results from oscillations $6-14$. The statistics are taken from equal intervals (two oscillations), so that the dashed, dotted, dash-dotted lines in in Figure 2 contains statistics from $0-2$, $2-4$, and $4-6$ oscillations respectively.

The transition region is not shown in this figure and the fully developed boundary layer exists from $x = 150$. Immediately after the oscillation starts, at $x = 250$, the skin friction starts to decrease. After six oscillations the resulting skin friction has converged to its converged steady value. A small overshoot can be detected since the skin friction is lower for oscillations $4-6$ than for $6-14$. This non-monotonic behaviour of the skin friction was also observed in channel flow simulations [4].

The drag reduction (DR) is calculated from

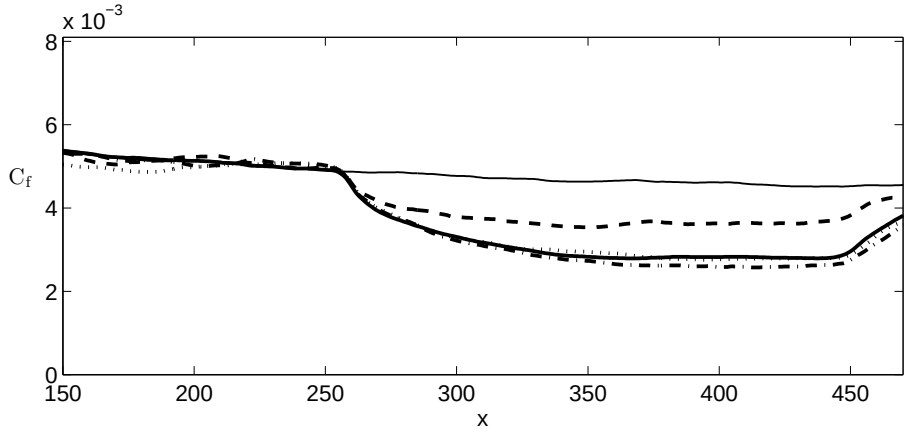

Figure 2. Skin friction after (- -) two oscillations; $(\cdots)$ four oscillations; $(- \cdot -)$ six oscillations. The thick solid line is C_f from the 6th to 14th oscillation. The thin solid line is C_f^0 from the unmanipulated boundary layer.

$$\mathrm{DR}(\%) = 100\frac{C_f^0 - C_f}{C_f^0}, \tag{16}$$

where C_f^0 is the skin friction of the reference case. For the DR calculation of case RES1, only the data from oscillations 6-14 is used.

The maximum DR is 40% and the value reported by Quadrio and Ricco [5] from DNS of channel flow with $T^+ = 100$ and $W_m^+ = 27$ is 44.7%. The formula given by equation (3) yields a value of 43% for these parameters. The Reynolds number based on the friction velocity in the uncontrolled channel and half the distance between the channel walls was $Re_\tau = 200$ in their simulations, while equation (3) is (explicitly) independent on Reynolds number.

In order to collect turbulence statistics a much longer (in time) simulation is needed, and it is only after a stationary mean flow has been obtained that the sampling should commence. Before running a longer simulation, a higher resolution given in Table (1) as the case RES2, was chosen. To reduce the simulation time a lower wall velocity was selected. For this case we choose $W_m^+ = 18$ while the period remains the same at $T^+ = 100$. In [5], the DR reported for the channel flow with $W_m^+ = 18$ is 39.1%, hence the difference in DR between the $W_m^+ = 18$ and $W_m^+ = 27$ is not great, while the gain in computational efficiency is tremendous. The results presented below will show that the DR remains similar (the DR reduces from 40% to 37%) for the lower wall velocity as compared to the higher wall velocity also in the boundary layer case.

In addition, the non-oscillating boundary layer flow was also calculated using the resolution RES2, and the comparison with the RES1 case is made in Figure 3. No significant difference between the two resolutions can be found. Furthermore, no difference in the velocity profiles from the two cases could be detected. In Figure 3, the transition region is included, and a sharp increase in C_f when turbulence is triggered at $x = 5$ can be noticed. The transition region extends until approximately $x = 150$, where the turbulence is fully developed.

To ensure time-independent statistics the sampling started at $t = 3600$ which is equal to approximately six periods of oscillations from the start ($t = 3000$) of the oscillations. A total of 5118 time units with oscillation constantly disturbing the flow were then simulated, which corresponds to 52 periods of oscillations. Hence,

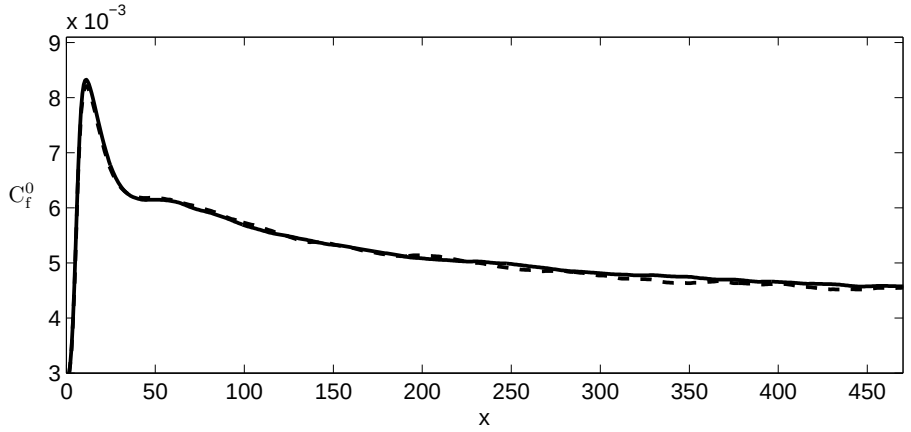

Figure 3. Skin friction for the unmanipulated boundary layer with (- -) RES1 and (—) RES2.

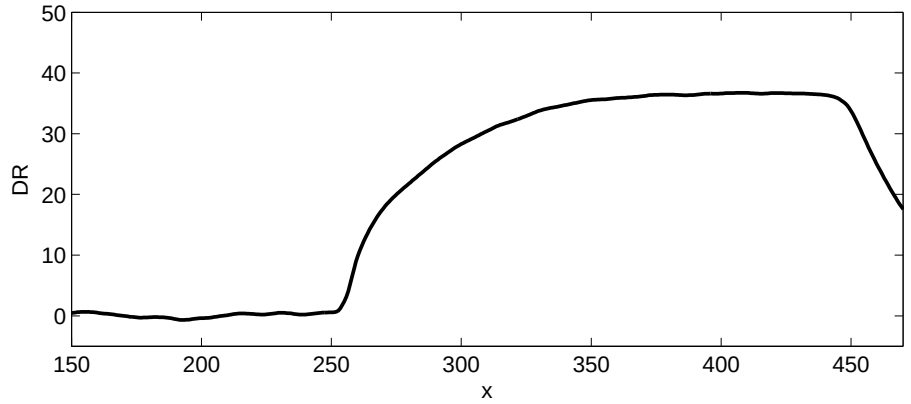

Figure 4. Drag reduction (in %) for case RES2.

most of the statistics presented in the remainder of this paper is taken over a time period of 52 oscillations (oscillation $6 - 58$). When dividing the statistics in two time intervals, no difference in the turbulence statistics could be found (see Figure 6b). The reason for the relatively long time taken for sampling is the behaviour of the Reynolds shear stress ($-\overline{uv}^+$) which will be discussed in the next section.

The maximum drag reduction for this case (RES2) is 36.8% which is slightly below the value for the channel flow geometry at 39.1% with the same parameters obtained by Quadrio and Ricco [5]. For a maximum wall velocity of $W_m^+ = 12$, the drag reduction was 32.8% in their simulation. Ricco & Wu [15] obtained a DR of 32% for $W_m^+ = 18$, but $T^+$was only 42 in that case. The Reynolds number based on the momentum thickness was higher in the experiment with a value of $Re_\theta = 1400$.

The value of DR obtained from equation (3) with the parameters as in the present study is 36.8%, exactly the value obtained from simulation data. The drag reduction over the useful part of the plate is shown in Figure 4.

The drag reduction behaves in a very similar manner to what was observed by Bogard et al. [11]. The increase in DR is rapid just after the onset of oscillation and increases less dramatically until saturated after approximately a distance of 100 in simulation units (δ^*), (the distance between $x = 250$ and $x = 350$). When scaled with wall units, the distance of rising DR is about 2200 which compares well with the experimental value of around 2000. The same distance was reported in Ricco & Wu [15]. When scaling the streamwise coordinate with δ^{99} at $x = 250$,

the distance from the beginning of the oscillation to the constant drag reduction at $x = 350$ is 10, which is roughly three times longer than the corresponding value in [11] which was reported as 3. However, the Reynolds number based on momentum thickness was 1400 in [11] while the present simulation was performed at a three times lower Reynolds number ($Re_\theta = 532$ at $x = 250$).

No upstream influence on the DR was detected that supports the observations by Choi et al. [10]. The lack of upstream influence in the present investigation could be due to the smooth transition between steady and moving wall used in the simulations, in contrast to the sharp edge used in experiments [10]. Ricco & Wu [15] reported that no upstream influence was detected in their experimental investigation.

In Quadrio and Ricco [4] it is argued that the start-up distance would be $6000 - 12000$ viscous lengths (based on the assumption on a convective velocity of $10u_\tau$). The present simulation and the experiments by Bogard et al. [11] and Ricco & Wu [15] seem to indicate that the transient length is not as long as estimated in [4]. Especially since our results coincides with the semi-empirical formula, equation (3), which is based on experimental evidence.

Our simulation results (referring to Figure 4) show a fairly constant DR for 90 simulation units ($350 - 440$), which corresponds to 9 boundary layer thicknesses or 2000 wall units. In the experiment reported in [15], the DR is constant for roughly 7 boundary layer thicknesses, mounting to 5000 wall units. In their case DR is 24% while equation (3) yields 28.1% for the parameters $W_m^+ = 11.3$ and $T^+ = 67$ used in their case. However, it may be that the constant value of the DR in these investigations are of a spatially quasi-steady type and will change further downstream. No simulation or experiment has been performed on a long enough domain to determine if the drag reduction changes further downstream. Nevertheless, the conclusion that can be drawn from the present simulation and the experiments reported in [11] and [15] regarding the spatial transients is that the distance from the onset of oscillation to a roughly constant DR is around $2000 - 2200$ based on wall units.

3.2. *Turbulence statistics*

In this section we only use the results from the RES2 (see Table 1) simulation. All parameters except the resolution and W_m were the same as in the RES1 simulation. The velocity profiles from the reference case and the oscillating boundary layer at $x = 400$ are shown in Figure 5a. The comparison is a direct confirmation of the profiles sketched by Choi & Clayton [12] and Choi [13]. They argued that a spanwise vorticity created by the periodic Stokes layer modifies the streamwise velocity profile. These arguments are further refined and explained in [18].

The velocity profile in wall scaling are shown in Figure 5b. The dashed line represents the velocity profile scaled with the actual u_τ and follows the linear profile ($u^+ = y^+$) close to the wall. When the same profile is scaled with u_τ^0 (the friction velocity from the non-oscillating boundary layer), the profile collapses with the reference profile in the outer region. In the small (due to the low Reynolds number) logarithmic region, the profile is shifted upward in the oscillating case. The subtle change in the logarithmic region is difficult to detect in experiments (see e.g. [9]), while it has been observed in channel flow simulation in [1] and [2].

The streamwise (u_{rms}^+) and normal (v_{rms}^+) velocity fluctuations are shown in Figure 6a together with the Reynolds shear stress ($-\overline{uv}^+$). Two curves are shown for each quantity (u_{rms}^+, v_{rms}^+ and $-\overline{uv}^+$). The profiles with larger values are from the reference case. Thus, a decrease in all Reynolds stresses are observed in Figure

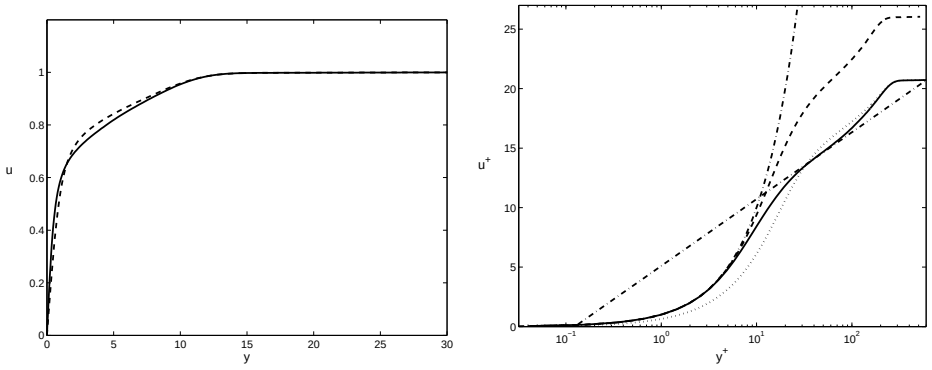

(a) (b)

Figure 5. Velocity profile at $x = 400$. a) (—) unmanipulated boundary layer; (- -) with oscillating wall. b) (—) unmanipulated boundary layer; (- -) oscillating wall scaled with actual u_τ; $(\cdots)$ oscillating wall scaled with u_τ^0; $(- \cdot -)$ $u^+ = y^+$ and $u^+ = \frac{1}{0.41} \ln y^+ + 5.1$.

6a, and the reduction of the peak values are 33%, 22% and 40% for u^+_{rms}, v^+_{rms} and $-\overline{uv}^+$ respectively. Compared to the experimental data in Laadhari et al. [8] who reported 45%, 34% and 50% for the three quantities, the present values are low, although the ratio between the different values seems to agree. On the other hand, values reported by Trujillo [9] was 15%, 25% and $20\% - 40\%$ (depending on whether the peak-to-peak values were used). Also Ricco & Wu [15] reported lower values at 14% for u^+_{rms} and 25% for $-\overline{uv}^+$ for two experiments with different W^+_m (9 and 18) and T^+ (83 and 42), but equal $D^+_m = 240$. Even though the values of the Reynolds stress reduction were equal in the two experiments in [15], they lead to different drag reduction of 25% and 32% respectively.

Also in DNS of channel flow, the general conclusion is that the decrease in $-\overline{uv}^+$ is greater than in u^+_{rms} and v^+_{rms}, see e.g. [4]. The greater reduction in Reynolds shear stress as compared to the *rms*-values is expected since the Reynolds shear stress is quadratic in the fluctuating velocity.

The u^+_{rms} for two streamwise positions ($x = 300$ and $x = 400$) are shown in Figure 6b. In the reference case there is not much difference in the profiles since the variation of the Reynolds number is small ($Re_\theta = 587$ and 690 respectively). In the oscillating case however, the development of the changing u^+_{rms} profile can be observed. At $x = 300$ the DR has not yet reached its final value (see Figure 4) and from the u^+_{rms} profile it can be seen that the inner part of the profile has adjusted while the outer part still follows the reference case profile. There is an overshoot in the reduction of u^+_{rms} since the peak of the profile at $x = 300$ is below the peak at $x = 400$. The phenomena of non-monotonous decay in the Reynolds stresses was also observed in the channel flow DNS by Quadrio and Ricco [4].

In addition, the statistics for u^+_{rms} at $x = 300$ have been taken from two roughly equally long time periods and are plotted together in Figure 6b. The lines are collapsing, thus indicating that the statistics is time independent. The two time intervals are denoted T1 and T2. T1 covers the oscillations $6 - 30$, while T2 covers oscillations $31 - 58$.

The streamwise and wall-normal velocity fluctuations scaled with actual friction velocity and the reference value u^0_τ are shown in Figure 7. For u^+_{rms} the scaling with actual u_τ does not result in a peak of the same value as for the reference case in contrast to the profile given in the experiment by Trujillo [9] at a Reynolds number of $Re_\theta = 1500$. This difference could be due to the lower Reynolds number

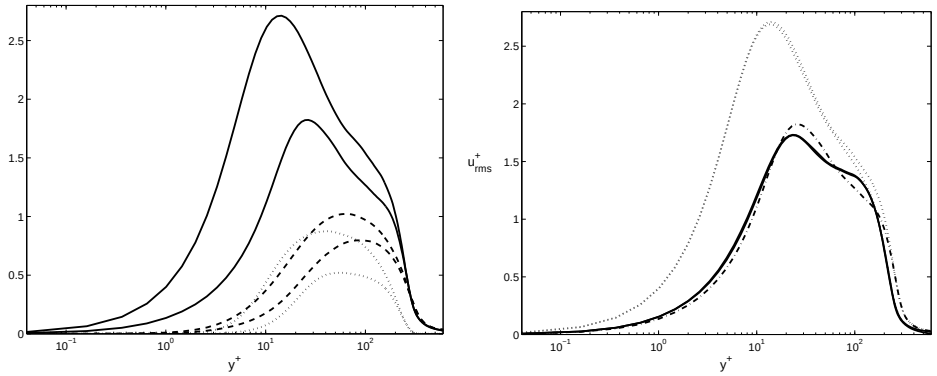

(a) (b)

Figure 6. a) (—) u^+_{rms}; (- -) v^+_{rms}; $(\cdots)$ $-\overline{uv}^+$; the higher curves are the unmanipulated boundary layer; the lower curves are for the oscillating wall case, scaled with u^0_τ. b) $(\cdots)$ u^+_{rms} profiles from the unmanipulated boundary layer at $x = 300$ (lower curve) and $x = 400$ (higher curve). (—) u^+_{rms} at $x = 300$ for the oscillating case (actually two curves for time intervals T1 and T2); $(- \cdot -)$ u^+_{rms} at $x = 400$ for the oscillating case, scaled with u^0_τ.

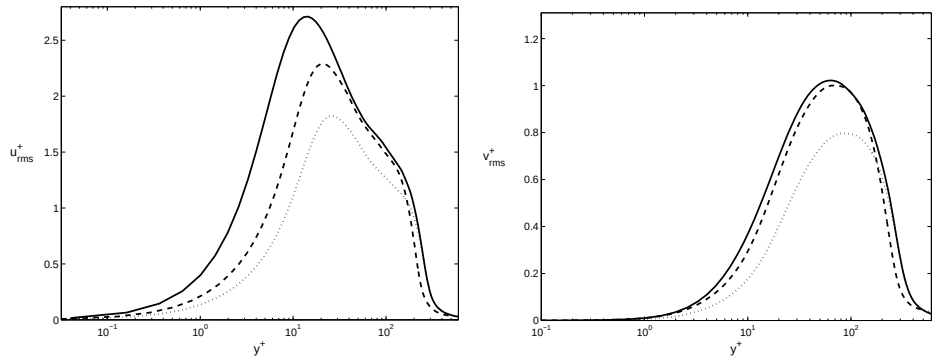

(a) (b)

Figure 7. a) Streamwise velocity fluctuations. b) Wall-normal velocity fluctuations. (—) reference case; (- -) oscillating wall scaled with actual u_τ; $(\cdots)$ oscillating wall scaled with u^0_τ.

in our simulation. On the other hand, channel flow simulations at a lower Reynolds number by Baron & Quadrio [2] showed that the peak value for the oscillating case even exceeds that of the unmanipulated channel when scaled with the actual u_τ. In the outer part of the boundary layer, the scaling with the u^0_τ causes the profiles from the two cases to collapse. For v^+_{rms}, the profiles in Figure 7b are very similar to the profiles given in Trujillo [9], for both scalings.

The profiles that deviates the most between different experiments are those obtained for the Reynolds shear stress. In the remainder of this section we will compare our results with experimental data and also try to come up with reasons for the differences between the different experiments and DNS data available.

Comparison of the Reynolds shear stress $(-\overline{uv}^+)$ profiles from three experiments is done in Figure 8a. An outer, second, peak is observed in the data from Trujillo [9] ($Re_\theta = 1500$; $W^+_m = 11.3$; $T^+ = 67$) and from (however less distinct) Ricco & Wu [15] ($Re_\theta = 1400$; $W^+_m = 9$; $T^+ = 83$). The present results show no such peak and is similar to the data in Laadhari et al. [8] ($Re_\theta = 950$; $W^+_m = 9.8$; $T^+ = 67$).

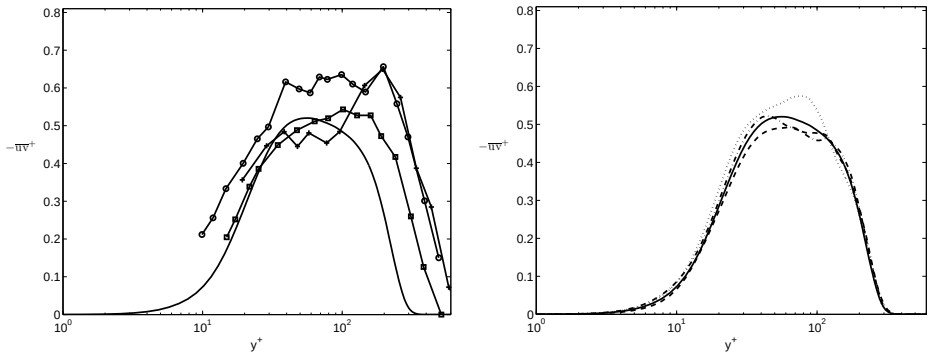

(a) (b)

Figure 8. $-\overline{uv}^+$ a) (—) Present simulation data at $x = 400$; (+) Trujillo [9]; (○) Ricco & Wu [15]; (□) Laadhari et al. [8]. b) (—) total statistics; (- -) statistics from oscillation $6 - 10$; $(\cdots)$ statistics from oscillation $20 - 25$; $(- \cdot -)$ statistics from oscillation $40 - 45$.

Furthermore, the DNS of channel flow by Quadrio and Ricco [4] do not reveal such features even though their transient data did exhibit second peak further up in the channel.

To investigate further we divided the statistics into ten segments, each containing approximately 4 to 5 cycles of oscillations. In Figure 8b the profiles obtained from oscillations $6 - 10$, $20 - 25$ and $42 - 47$ together with the converged total statistics curve obtained from all 52 oscillations are shown. These particular profiles were chosen because they deviate the most from the mean profile. A tilting of the profile towards larger y^+ values can be seen in the profile taken from $20 - 25$ oscillations, and a double peak is visible in both the profiles taken from oscillations $6 - 10$ and $42 - 47$ respectively. The shape of the curves depends on the time interval chosen for the statistics and our choice of 5 periods is arbitrary, but the point is that the statistics is sensitive to the time chosen for collection (sampling) of statistics. In [15] a sampling time of 2000 wall units is mentioned. However, the required sampling time for the statistics to converge might vary with the Reynolds number. In our case the error (compared with the full statistics from all 52 oscillations) in the maximum Reynolds shear stress is about 8% when data from only five oscillations is considered. When the 25 and 28 oscillation data (denoted T1 and T2 earlier) are used, the error reduces to 0.8%. This error is hardly visible when the profiles are plotted together in a graph such as Figure 8b.

In [4] it was suggested that the lower DR results in experiments compared to simulation occurred due to the neglect of transients. The present results point to the fact that also the length of time used for sampling of statistics plays a role. Too short time allocated for sampling might explain the discrepancies in the Reynolds stress profiles obtained by different experiments and simulations.

Neither the velocity profiles nor the u^+_{rms} and v^+_{rms} profiles show the same sensitivity on sampling time.

3.3. *Reynolds stress budget*

The transport equations for the Reynolds stress tensor $R_{ij} = \overline{u_i u_j}$ read

$$\frac{\mathrm{D}R_{ij}}{\mathrm{D}t} \equiv \left(\frac{\partial}{\partial t} + U_j \frac{\partial}{\partial x_j}\right) R_{ij} = \mathcal{P}_{ij} - \varepsilon_{ij} + \Pi_{ij} + G_{ij} + D_{ij} + T_{ij} \qquad (17)$$

where

$$\mathcal{P}_{ij} \equiv -\overline{u_i u_k}\frac{\partial U_j}{\partial x_k} - \overline{u_j u_k}\frac{\partial U_i}{\partial x_k}, \tag{18a}$$

$$\varepsilon_{ij} \equiv 2\nu\overline{u_{i,k}u_{j,k}}, \tag{18b}$$

$$D_{ij} \equiv \frac{\partial}{\partial x_k}\left(\nu R_{ij,k}\right), \tag{18c}$$

$$\Pi_{ij} \equiv \frac{1}{\rho}\left(\overline{p\frac{\partial u_i}{\partial x_j} + p\frac{\partial u_j}{\partial x_i}}\right), \tag{18d}$$

$$G_{ij} \equiv -\frac{\partial}{\partial x_k}\left(\frac{1}{\rho}\overline{u_j p}\delta_{ik} + \frac{1}{\rho}\overline{u_i p}\delta_{jk}\right), \tag{18e}$$

$$T_{ij} \equiv -\frac{\partial}{\partial x_k}\overline{u_i u_j u_k}. \tag{18f}$$

Here $\mathcal{P}_{ij}$ is the production due to mean field gradients, whose trace ($\mathcal{P}_{ii}$) represents twice the production of turbulent energy, the transfer of energy from the mean flow to the turbulent fluctuations.

ε_{ij} is the dissipation rate tensor, and D_{ij} is the diffusion tensor. They both represent viscous effects, but whereas D_{ij} is a molecular diffusion term acting to even out the turbulent stresses by spatial redistribution, ε_{ij} act as a destruction term of turbulent energy (and stresses).

Π_{ij} is the pressure-strain rate correlation tensor, which is traceless and represents inter-component transfer between Reynolds stress terms. G_{ij} is the divergence of the pressure-velocity correlation, and represents transport driven by pressure fluctuations.

T_{ij} is the divergence of the triple correlation tensor, acting as a spatial redistribution term.

See [26] for examples of budgets for different components in various geometries. In Figure 9 the budget for $R_{11} = u_{rms}^2$ in wall units (scaled with ${u_\tau}^4/\nu$) is presented. Data are taken from $x = 400$. The solid lines in both figures represent the reference case, and the results are identical to those obtained by Komminaho & Skote [26]. In Figure 9a, the reference case is compared to the wall-oscillating boundary layer with the scaling based on the actual u_τ, and in Figure 9b, all quantities are scaled with u_τ^0 from the reference case.

The maximum of the production shifts outward and the dissipation decreases near the wall in both scalings. The dissipation in the scaling with actual u_τ exceeds the reference case profile above $y^+ = 7$, while it remains less than the reference case when scaled with u_τ^0. The viscous diffusion also decreases near the wall for both scalings, but more details are available when scaling with actual u_τ is used since the values are larger.

The maximum of the production decreases more than 50% in the reference scaling, while the maximum value of 0.5 is retained when the production scaled with the actual u_τ. The value of 0.5 can be obtained by integrating the stream-wise momentum equation once, and multiplying with $\frac{dU^+}{dy^+}$. By neglecting the advection term and assuming wall similarity, we obtain the following relation for the turbulence production:

$$\mathcal{P}_{11} \equiv -2\frac{\overline{uv}}{u_\tau^2}\frac{\mathrm{d}U^+}{\mathrm{d}y^+} = 2\frac{\mathrm{d}U^+}{\mathrm{d}y^+}\left(1 - \frac{\mathrm{d}U^+}{\mathrm{d}y^+}\right). \tag{19}$$

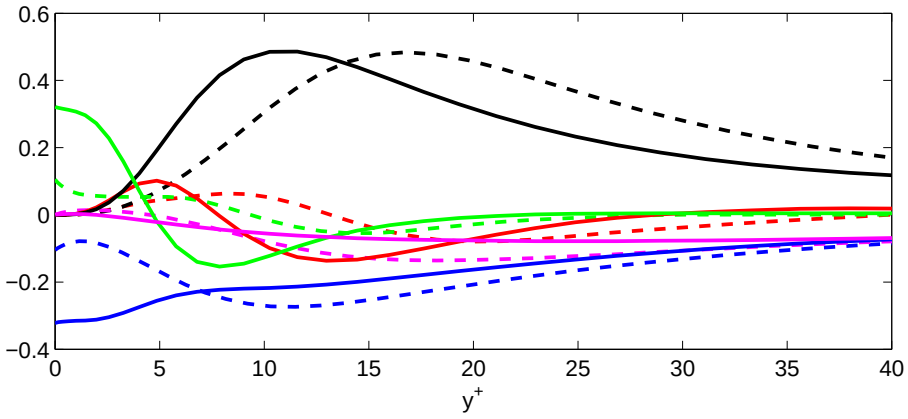

(a)

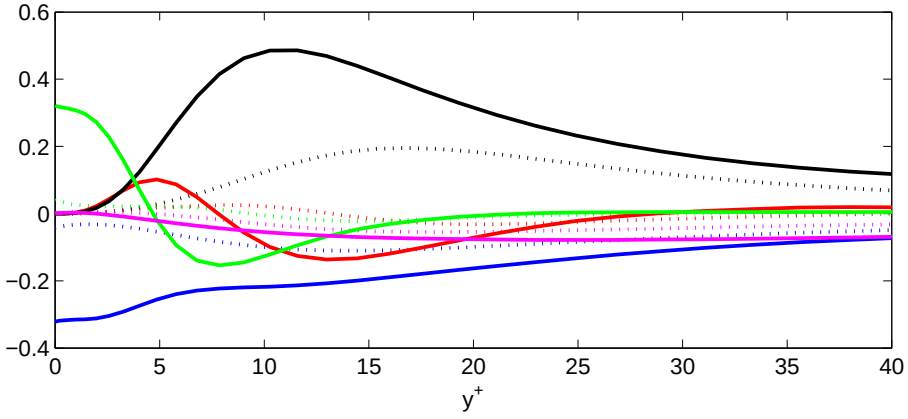

(b)

Figure 9. Budget for R_{11} at = 400. (—) unmanipulated boundary layer; a) (- -) oscillating wall scaled with actual u_τ; b) $(\cdots)$ oscillating wall scaled with u_τ^0. Colour coding for the different terms: $\mathcal{P}_{11}$; ε_{11}; D_{11}; Π_{11}; T_{11}.

From the above relation it follows that the maximum of $\mathcal{P}_{11}$ is 0.5 occurring at a position where $\mathrm{d}U^+/\mathrm{d}y^+ = 0.5$

The changes in the budget terms for the oscillating case compared to the reference boundary layer budget are similar to the observation of channel flow data in [2]. Also in the large-eddy simulation of a three-dimensional boundary layer by Kannepalli & Piomelli [20] similar behaviour can be found, especially the form of dissipation near the wall follows closely the present profile, at least in the beginning of the shear driven region.

4. Conclusion

The spatial development of drag reduction is essentially identical to experimental findings, when the streamwise coordinate is scaled with wall units.

The drag reduction obtained from the simulation (36.8% for a maximum wall speed of 18, and period of 100 in wall units) was identical to the value obtained from a semi-empirical formula.

The decrease in the peak streamwise and normal velocity fluctuations were 33% and 22% respectively, while the peak Reynolds shear stress decreased with 40%.

For second order statistics, especially the Reynolds shear stress, sampling time must be longer than for velocity profiles. For a low Reynolds number considered here, we have shown that around 25 periods is sufficient (about half the total number of oscillations the turbulent boundary layer was admitted to experience during the sampling for statistics). This number might of course be Reynolds number dependent. The strong variation of the Reynolds shear stress profiles found in earlier experiments of turbulent boundary layers over an oscillating wall was found to be at least partially reproduced with the present direct numerical simulations by varying the length of the sampling time (for producing turbulence statistics). On the other hand, the fully converged profile did not exhibit any of the deviating shapes found in experimental data and resembled more the profile obtained numerically for channel flow geometry.

References

[1] W.J. Jung, N. Mangiavacchi, and R. Akhavan, *Suppression of turbulence in wall-bounded flows by high-frequency spanwise oscillations*, Phys. Fluids A 4 (1992), pp. 1605–1607.

[2] A. Baron, and M. Quadrio, *Turbulent drag reduction by spanwise wall oscillations*, Appl. Sci. Res. 55 (1996), pp. 311–326.

[3] J.I. Choi, C.X. Xu, and H.J. Sung, *Drag reduction by spanwise wall oscillation in wall-bounded turbulent flows*, AIAA J. 40 (2002), pp. 842–850.

[4] M. Quadrio, and P. Ricco, *Initial response of a turbulent channel flow to spanwise oscillation of the walls*, J. Turbul. 4 (2003).

[5] M. Quadrio, and P. Ricco, *Critical Assessment of Turbulent Drag Reduction Through Spanwise Wall Oscillations*, J. Fluid Mech. 521 (2004), pp. 251–271.

[6] C.X. Xu, and W.X. Huang, *Transient response of Reynolds stress transport to spanwise wall oscillation in a turbulent channel flow*, Phys. Fluids 17 (2005).

[7] P. Ricco, and M. Quadrio, *Wall-oscillation conditions for drag reduction in turbulent channel flow*, Intl J. Heat Fluid Flow 29 (2008), pp. 601–612.

[8] F. Laadhari, L. Skandaji, and R. Morel, *Turbulence reduction in a boundary layer by a local spanwise oscillating surface*, Phys. Fluids 6 (1994), pp. 3218–3220.

[9] S.M. Trujillo, D.G. Bogard, and K.S. Ball, *Turbulent boundary layer drag reduction using an oscillating wall*, AIAA Paper 97-1870 (1997).

[10] K.S. Choi, J.R. DeBisschop, and B.R. Clayton, *Turbulent boundary-layer control by means of spanwise wall oscillation*, AIAA J. 36 (1998), pp. 1157–1163.

[11] D.G. Bogard, K.S. Ball, and E. Wassen, *Drag Reduction for Turbulent Boundary Layer Flows Using an Oscillating Wall*, AFOSR, The university of Texas at Austin, 2000.

[12] K.S. Choi, and B.R. Clayton, *The mechanism of turbulent drag reduction with wall oscillation*, Intl J. Heat Fluid Flow 22 (2001), pp. 1–9.

[13] K.S. Choi, *Near-wall structure of turbulent boundary layer with spanwise-wall oscillation*, Phys. Fluids 14 (2002), pp. 2530–2542.

[14] G.M. Di Cicca, G. Iuso, P.G. Spazzini, and M. Onorato, *Particle image velocimetry investigation of a turbulent boundary layer manipulated by spanwise wall oscillations*, J. Fluid Mech. 467 (2002), pp. 41–56.

[15] P. Ricco, and S. Wu, *On the effects of lateral wall oscillations on a turbulent boundary layer*, Exp. Therm. Fluid Sci. 29 (2004), pp. 41–52.

[16] P. Ricco, *Modification of near-wall turbulence due to spanwise wall oscillations*, J. Turbul. 5 (2004), pp. 1–18.

[17] K.S. Choi, and M. Graham, *Drag reduction of turbulent pipe flows by circular-wall oscillation*, Phys. Fluids 10 (1998), pp. 7–9.

[18] G.E. Karniadakis, and K.S. Choi, *Mechanisms on transverse motions in turbulent wall flows*, Annu. Rev. Fluid Mech. 35 (2003), pp. 45–62.

[19] M. Quadrio, and S. Sibilla, *Numerical simulation of turbulent flow in a pipe oscillating around its axis*, J. Fluid Mech. 424 (2000), pp. 217–241.

[20] C. Kannepalli, and U. Piomelli, *Large-eddy simulation of a three-dimensional shear-driven turbulent boundary layer*, J. Fluid Mech. 423 (2000), pp. 175–203.

[21] M. Chevalier, P. Schlatter, A. Lundbladh, and D.S. Henningson, *SIMSON — A Pseudo-Spectral Solver for Incompressible Boundary Layer Flows*, Technical report, TRITA-MEK 2007:07, KTH, Stockholm, Sweden, 2007.

[22] M. Skote, D.S. Henningson, and R.A.W.M. Henkes, *Direct numerical simulation of self-similar turbulent boundary layers in adverse pressure gradients*, Flow, Turbulence and Combustion 60 (1998), pp. 47–85.

[23] M. Skote, and D.S. Henningson, *Direct numerical simulation of a separated turbulent boundary layer*, J. Fluid Mech. 471 (2002), pp. 107–136.

[24] A.H. Herbst, and D.S. Henningson, *The influence of periodic excitation on a turbulent separation bubble*, Flow, Turbulence and Combustion 76 (2006), pp. 1–21.
[25] P. Schlatter, R. Orlu, Q. Li, G. Brethouwer, J.H.M. Fransson, A.V. Johansson, P.H. Alfredsson, and D.S. Henningson, *Turbulent boundary layers up to Re-theta=2500 studied through simulation and experiment*, Phys. Fluids 21 (2009).
[26] J. Komminaho, and M. Skote, *Reynolds stress budgets in Couette and boundary layer flows*, Flow, Turbulence and Combustion 68 (2002), pp. 167–192.